

ASSEMBLY CONFORMITY OF STRUCTURE GROWTH: FOSSIL VERSUS NORMAL GROUPS OF GALAXIES

ZACK LI¹ AND RENYUE CEN¹

¹*Department of Astrophysical Sciences
Princeton University
Peyton Hall, 4 Ivy Lane
Princeton NJ 08544, USA*

ABSTRACT

Using a semi-analytic method calibrated to the global star formation history and the stellar mass function at $z = 0$, we attempt to understand the most stellar deficient galaxy groups. We argue such groups are a kind of fossil group (FGs) — in comparison to the normal groups of galaxies, they assemble both halo and stellar mass earlier. We find there is a central galaxy and satellite conformity between these FGs and normal groups: centrals and satellites in the former form earlier and more stellar deficient than their counterparts of the latter. We term this effect “Assembly Conformity” of dark matter halos. This effect accounts for about 70% of the difference in stellar content between FGs and normal groups. When split by the peak redshift for the star formation rate of a group, the mass functions of satellite halos on either side of the peak redshift are found to be indistinguishable between FGs and normal groups, indicating a self-similarity of halo assembly with respect to the peak. The “baryonic environmental” effect due to ram-pressure and gas heating accounts for about 30% of the difference in stellar content. While the total stellar mass of FGs is lower than that of normal groups, we predict that the mass of the brightest central galaxy of FGs is, on average, higher than that of normal groups. We also predict that in the central galaxies of FGs, there is a negative stellar age gradient from the center outward, where the opposite is expected for those in normal groups.

arXiv:2007.11021v1 [astro-ph.GA] 21 Jul 2020

1. INTRODUCTION

Fossil groups (FGs) are galaxy systems which have extended X-ray halos and a single bright, central galaxy which dominates the system’s optical luminosity. Such groups have been long conjectured to occur when the largest satellites of an old and isolated group have merged into the central galaxy through dynamical friction (Barnes 1989; D’Onghia et al. 2005; Dariush et al. 2007). Direct evidence for this picture is still lacking, but there is allure to a connection between group morphology and history, and such relaxed groups would be a useful laboratory for studying galaxy evolution while normalizing for recent mergers.

Although the original motivation was to find early-forming systems, selection criteria for FGs typically rely on the gap in optical magnitude between the first and second brightest galaxies. This selection method stems from the idea that repeated mergers in isolated and relaxed systems should make the central galaxy brighter, while simultaneously depleting the population of bright satellites. Jones et al. (2003) established the conventional observational definition for FGs, identifying FGs as extended sources with X-ray luminosity $L_X \geq 10^{42} h_{50}^{-1}$ ergs s⁻¹ and an *R*-band magnitude gap $\Delta m_{12} \geq 2.0$ mag between their central galaxy and the second brightest object within half the projected virial radius.

Despite a conjectured formation scenario which departs from ordinary hierarchical assembly, the only observed properties of FGs which differ significantly from groups of the same halo mass relate to their brightest group or cluster galaxy (BCG). There is a consensus among observers that FG BCGs are special, and in particular brighter than those of typical groups (Harrison et al. 2012), dominating the total optical luminosity of the cluster. This result follows from the magnitude-gap selection criteria, but excludes groups which have typical stellar masses but have fewer massive satellites and more low-mass satellites. Bharadwaj et al. (2016) find that the X-ray peak is located near the dominant elliptical in all seventeen FGs they studied, further supporting the existence of a connection between FG BCGs and overall group properties. Raouf et al. (2019) find substantial differences in the color of GAMA brightest group galaxies, using SED-fitting of GAMA groups selected with a magnitude gap and BCG offset, suggesting differences in the central stellar populations of relaxed groups relative to typical groups.

There is evidence that FGs have stellar population properties consistent with typical groups. La Barbera et al. (2009) study 25 FGs and find similar ages, metallicities, and α -enhancements as bright field ellipticals.

Egenthaler & Zeilinger (2013) measure metallicity gradients of six central galaxies in FGs and find generally negative metallicity gradients similar to those found in cluster ellipticals of similar mass. Zibetti et al. (2009) study a sample of six FG and find the cumulative substructure distribution functions (CSDFs) of FGs are consistent with those of typical clusters. Zarattini et al. (2016) find galaxy substructures in twelve systems and find a similar fraction of substructure as detected in non-fossil clusters. FGs also appear in both poor and rich environments (Pierini et al. 2011; Adami et al. 2012). Similarly, scaling relations for X-ray luminosity and temperature of FGs match those of non-FGs (Khosroshahi et al. 2007). Likewise, Trevisan et al. (2017) find no trends in stellar population properties like age, abundances, metallicities, and star formation histories of 550 SDSS groups with respect to the magnitude gap.

There is some debate about whether FGs are less bright in the optical than typical groups at fixed halo mass. Early observations reported halo mass-to-light ratios which were a factor of 2-3 higher than typical groups (Vikhlinin et al. 1999; Yoshioka et al. 2004; Khosroshahi et al. 2007), but these studies often involved only a handful of systems in their samples. Recent observations with larger sample sizes sometimes corroborate this factor of 2-3 (Proctor et al. 2011; Miller et al. 2012; Khosroshahi et al. 2014). However, other studies (Voevodkin et al. 2010; Harrison et al. 2012; Kundert et al. 2015) find no difference between optical and X-ray data, and argue that earlier works had inhomogeneous samples or selection effects.

These disagreements may come from issues with selection criteria, as samples selected through the magnitude gap suffer from both false positives and incompleteness for early-forming systems. Systems which assemble early, but are not completely isolated, can be excluded from the FG sample if they randomly have a moderately bright galaxy in the process of merging. Conversely, systems that randomly have fewer bright satellites can be included in this FG sample, even if they did not form early. Dariush et al. (2010) propose an alternate definition involving the gap between the first and fourth brightest galaxies to avoid excluding FGs with a few bright satellites, but find that both definitions fail to find the majority of early-forming systems. They also find that the FG definition is highly transient, with 90% of FGs becoming non-FGs after ~ 4 Gyr.

Possibly also due to these selection issues, there exists evidence for inhomogeneity of baryonic properties within the FG population. Proctor et al. (2014) found substantial differences between the age and metallicity gradients of two FGs with similar morphology, luminos-

ity, color, and kinematics, and suggest that FGs do not have homogeneous star formation histories. [Bharadwaj et al. \(2016\)](#) investigated the gas dynamics of FGs and found cool cores but a lack of a universal temperature profile, with some of the expected features of relaxed cool-core objects missing in low-temperature examples.

Theoretical work on the origin of FGs generally agree that the appearance of an optical gap is a transient phenomenon ([von Benda-Beckmann et al. 2008](#); [Dariush et al. 2010](#); [Kundert et al. 2017](#)). However, there is some disagreement about whether FGs really form earlier than typical groups, and whether the environment is important in FG formation ([D’Onghia et al. 2005](#); [Díaz-Giménez et al. 2011](#); [Cui et al. 2011](#)). Studies which suggest a connection between the central galaxy and the mass assembly history ([Khosroshahi et al. 2017](#); [Raouf et al. 2018](#)) support the idea that the magnitude gap is a good proxy for assembly history.

In this paper, we study how the low stellar mass tail of galaxy groups at a given halo mass at $z = 0$, which we define as the fossil groups (FGs), become stellar-mass deficient. We show, by a systematic dissection of involved processes, that large scale gravitational growth (i.e., dark matter) physics plays the chief role in determining the stellar mass of a group of galaxies. In particular, we show that both the primary progenitor of a group, i.e., the trunk of the merger tree of a group, and the branches and leaves of the merger tree, display assembly conformity in the sense that FGs and their building blocks have, on average, a higher assembly redshift than normal groups and their building blocks of the same halo mass at $z = 0$. In contrast, the overall mass distribution of constituent halos and subhalos in the two types (FGs versus normal) of groups over the entire merger trees are very similar.

We demonstrate that the large scale gravitational effects of assembly conformity cause the main progenitor and massive subhalos of FGs to enter hot mode accretion at a higher redshift than their counterparts of normal groups, shutting out the main progenitor and their massive subhalos of the former from the opportunity to form stars. This process leads to lower stellar content in FGs than in normal groups. Satellite galaxies that are not massive enough to be self-quenching still experience suppressed star formation from these gravitational processes, due to the environmental effects of massive neighbors. This primarily baryonic environmental effect acts in the same way as the gravitational environment effect above, but plays a secondary role in reducing stellar mass in FGs.

From the viewpoint of a superposition of waves of a random gaussian density field, the physical picture is

that the individual density peaks producing the FG primary progenitor and subhalos tend to be higher density than in normal groups, although the overall peak height at the group scale is similar since we select for a narrow mass range at $z = 0$ in our study. While this finding itself is new and subtle, it is in some way similar to the large-scale correlation among neighboring halos at large distances noted by [Hearin et al. 2016](#).

The outline of the paper is as follows. A description of a physical model for star formation is given in §2.1. The results are presented in §3, followed by conclusions in §4.

2. METHODS

2.1. Star Formation Model

Galaxy formation is complicated. One can try directly simulating the dark matter and gas physics using massive hydrodynamic simulations (i.e. [Vogelsberger et al. 2020](#)), but these still require parameterizing well-known but poorly constrained processes such as feedback processes from super-massive black growth (i.e. [Katz 1992](#); [Springel 2005](#); [Crain et al. 2009](#); [Schaye et al. 2010](#); [Vogelsberger et al. 2014](#); [Pillepich et al. 2018](#)). One can sacrifice predictive power for cheaper computational expenses using a more phenomenological approach on dark matter-only simulations, where one uses a set of parameters to model the physical processes thought to be relevant for galaxy formation. These are typically referred to as semi-analytic models (SAMs) and process merger trees from N-body simulations into baryonic predictions (i.e. [Kauffmann et al. 1993](#); [Somerville & Primack 1999](#); [Bower et al. 2006](#); [Benson 2012](#); [Henriques et al. 2015](#); [Raouf et al. 2017](#)).

We follow in the direction of this semi-analytic method, by implementing star formation in halo catalogs extracted from massive N-body simulation, creating a simplified model intended to provide physical understanding. This allows us to easily vary physical effects like the environmental suppression of star formation, which would be much more difficult with the expensive hydrodynamic approach. By using a simplified model based on the merger trees, we can draw clear conclusions between our modeling and our results on fossil group formation. We use the BolshoiP N-body simulations ([Trujillo-Gomez et al. 2011](#); [Klypin et al. 2011, 2016](#)) which has a box size of $0.25 h^{-1}$ Gpc and 2048^3 particles, with particle masses of $1.5 \times 10^8 h^{-1} M_{\odot}$ and a spatial resolution of $1 h^{-1}$ kpc comoving. The initial conditions are generated with cosmological parameters consistent with [Planck Collaboration et al. \(2014\)](#). We make a reasonable assumption that the gravitational dynamics of galaxy group size halos are not signifi-

cantly impacted by baryonic physics, so merger trees from simulations containing only dark matter are sufficient to model the growth and merger history of halos pertaining FGs and their counterparts. We confine the number of parameters to formulate the baryonic physics to the bare minimum, by focusing only on the most important known processes and aiming for physically motivated implementations. Our model is less complicated than the semi-analytic models used previously for the study of FGs (Dariush et al. 2007; Díaz-Giménez et al. 2011; Gozaliasl et al. 2014; Kanagusuku et al. 2016) or the computationally costly treatments of star formation involving hydrodynamics (Cui et al. 2011; Kundert et al. 2017). Using this model, we reproduce (see Section 3.4) a relatively weak connection between magnitude gap and group age found in i.e. Dariush et al. 2010 and Raouf et al. 2014.

We now describe the key elements of our model.

Normalization of star formation rate—We parametrize the halo-dependent star formation rate (SFR) in terms of the halo mass and the halo’s dynamical time, and set the overall normalization with a multiplicative constant c_* . That is,

$$\dot{M}_* = c_* H(M_h) K(M_h) M_h / t_{\text{dyn}}, \quad (1)$$

where M_h is halo mass, t_{dyn} the dynamical time of the halo. Here, two functions, $H(M_h)$ and $K(M_h)$, have been inserted to treat the physics of cold and hot gas accretion onto halos and supernova (and photoheating) feedback effects, respectively, as described next.

Hot-Cold Accretion Dichotomy—We represent the hot-cold accretion dichotomy with a characteristic transition halo mass M_c such that star formation in halos with masses $M_h > M_c$ is quenched due to gravitational heating. We implement this with a smooth step function in terms of the log halo mass,

$$H(x) = \frac{1}{1 + e^{-kx}}. \quad (2)$$

We use $x = \log_{10} M_h / M_c$ and $\log_{10} M_c / M_\odot = 12.5 + 0.1(z - 2)$ in our fiducial model, with a width $k = 1$, consistent with results from detailed hydrodynamic simulations (Kereš et al. (2009)). Thus, we use two parameters to describe the hot-cold accretion dynamics.

Environmental Effect—Gas accretion and dynamics in galaxies in the vicinity of massive halos with hot, extended atmospheres are subject to twin effects due to ram-pressure stripping and cold gas supply shortage. These environment effects are well known, seen in detail in cosmological hydrodynamic simulations. We parameterize this effect, based on insight gained in hydro

simulations (e.g., Cen 2014), by suppressing star formation in galaxies located within three virial radii of halos with hot accretion, with the suppression equal to $H(x)$ in Eq (2), where the massive neighbor halo in this case is the most massive halo with hot atmosphere that encloses the halo in question within the three virial radii of the former. There is ample observational evidence for such shock heating effects around clusters extending to a few virial radii (i.e. Balogh et al. 1999; Wetzel et al. 2012; Bahé et al. 2013; Haines et al. 2015).

Supernova Feedback—We model supernova feedback using a redshift-dependent velocity dispersion cutoff $\sigma_c(z)$, below which star formation is suppressed. We use a smooth step function as in Equation 2 with $x = \sigma_v / [(1 + z)\text{km/s}] - 25$, where σ_v is 1-d velocity dispersion of the halo, and $k = 0.2$. Here, we also use two parameters to describe the collective feedback due to supernovae. We considered adding feedback from photoheating of the intergalactic medium due to reionization, which is relevant at high redshift. We found that the negative feedback effect due to photoheating is subdominant to that of supernova feedback based on simple physical considerations and hence is not included in our treatment.

In summary, we use a total of five parameters (one for overall normalization of star formation efficiency, two for cold-hot accretion and environmental effects, and two for supernova feedback effects). We implicitly assume that during mergers, the descendant halo receives all of the stars of the merging halos, as the contribution of the ejected stars, seen for example as intra-cluster light mounts up to order of 10-20%, still smaller fractions in groups and poorer environments (Krick & Bernstein 2007). We apply a simple suppression of star formation at high halo mass to match observations. This could physically arise from processes such as AGN feedback or gravitational shock heating, but we keep the prescription simple due to the relatively poorly understood underlying physics.

Optimizing Physics Modeling Parameters—The parameters in our star formation model, as detailed above, are then optimized by matching two key observables – the star formation history of the universe and the galaxy stellar mass function at $z \sim 0$, shown in the right and left panels of Figure (1), respectively. Despite the small number of parameters employed, we obtain acceptable agreement with observations without sacrificing understanding.

2.2. Definition of Fossil Groups

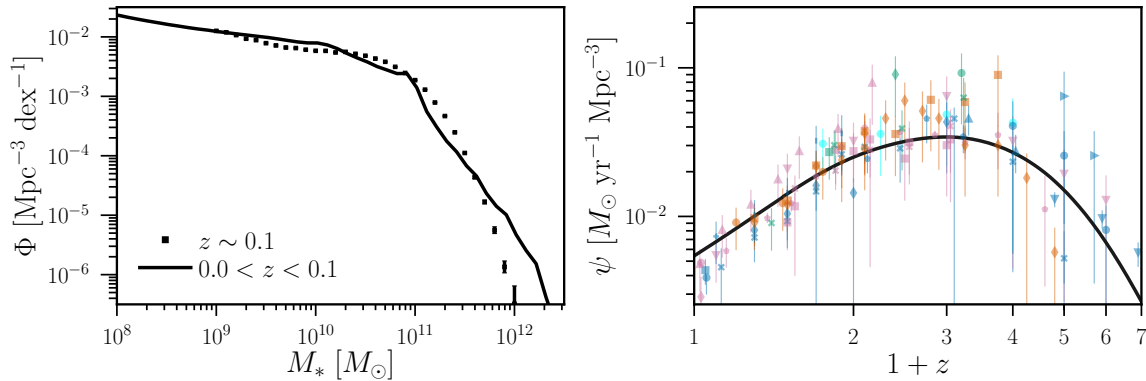


Figure 1. Left panel shows the stellar mass function at $z=0.1$ from observations (black squares, Moustakas et al. (2013)) and our model (black curve). Right panel shows the SFR density as a function of redshift (Madau plot) from observations (symbols) and our model (black curve). Observational data sources and their symbols are as follows. **UV (blue):** Wyder et al. (2005) (●), Schiminovich et al. (2005) (◆), Robotham & Driver (2011) (■), Cucciati et al. (2012) (×), Dahlen et al. (2007) (★), Reddy & Steidel (2009) (▲), Bouwens et al. (2012a,b) (▼), Schenker et al. (2013) (◀), Yoshida et al. (2006) (▶), Salim et al. (2007) (+), Ly et al. (2011b) (◆), van der Burg et al. (2010) (●), Zheng et al. (2007) (|). **IR (pink):** Sanders et al. (2003) (●), Takeuchi et al. (2003) (◆), Magnelli et al. (2011) (■), Magnelli et al. (2013) (×), Gruppioni et al. (2013) (★), Rujopakarn et al. (2010) (▲), Le Borgne et al. (2009) (▼); **H- α (green):** Tadaki et al. (2011) (●), Shim et al. (2009) (◆), Ly et al. (2011a) (■), Sobral et al. (2013) (×). **UV+IR (cyan):** Kajisawa et al. (2010) (●); **Radio (orange):** Smolčić et al. (2009) (●), Dunne et al. (2009) (◆), Karim et al. (2011) (■).

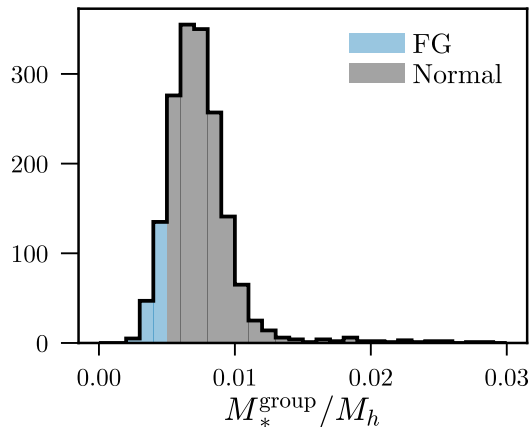


Figure 2. The probability distribution function of stellar to halo ratios of groups of halo masses in the range $10^{13.4}M_{\odot} < M_h < 10^{13.6}M_{\odot}$. Our standard method to select out low stellar content, FGs is shown by the cyan portion of the distribution, corresponding to a fraction is $\sim 10\%$ of all groups in the indicated halo mass range.

We define fossil groups in this paper based on the ratio of stellar mass to halo mass. Compared to the various fossil identification methods based on magnitude gaps between the brightest galaxy and its satellites, this definition is less sensitive to the timing within the merger process that is ubiquitous in the hierarchical growth process of halos. Let $\langle M_*^{\text{group}}/M_h \rangle$ be the ratio of total stellar mass to halo mass, averaged over all groups with halo mass $M_h = 10^{13.4} - 10^{13.6}M_{\odot}$ at $z = 0$. A FG is

defined to satisfy the following equation:

$$M_*^{\text{group}}/M_h < 0.5 \langle M_*^{\text{group}}/M_h \rangle. \quad (3)$$

This definition, in addition to having the advantage of being relatively immune to the exact timing of merger processes that may render the ranking based definition unstable, is motivated by our desire of making the comparative statements robust, not subject to uncertainties in the absolute values of the multiplicative parameters, such as c_* , in the model. Although the halo mass range of real FGs may be larger than adopted here, we choose a narrower range of halo masses to avoid possible mass segregation effects of the two classes of groups, to more cleanly gain physical insight. We define the “normal” set to be the remaining groups in the same halo mass range $10^{13.4}M_{\odot} < M_h < 10^{13.6}$, meeting the condition

$$M_*^{\text{group}}/M_h \geq 0.5 \langle M_*^{\text{group}}/M_h \rangle. \quad (4)$$

We show these two samples in Figure 2 with respect to their stellar mass distribution, and highlight our selection of the most stellar-mass-deficient groups. For the selected mass range $M_h = 10^{13.4} - 10^{13.6}M_{\odot}$ at $z = 0$, the overall distribution has a mean stellar-to-halo mass ratio of ~ 0.007 with a standard deviation of ~ 0.002 . Figure 3 shows the halo mass distributions of the two groups are similar.

To facilitate an assessment of selection methods based on luminosity gaps between ranking galaxy members in a group, we use the ratio in stellar masses as a proxy for

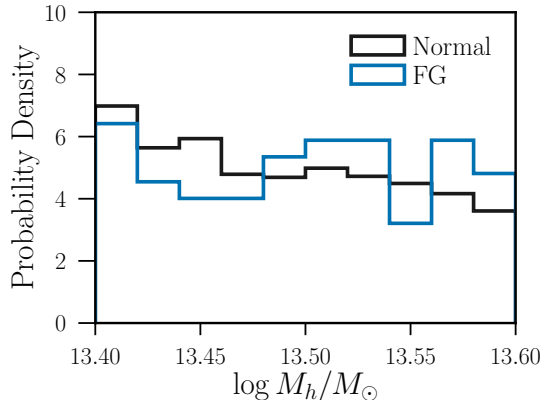


Figure 3. The halo mass probability distributions resulting from our selection. Within this narrow mass range used for the analysis ($13.4 < \log_{10} M_h/M_\odot < 13.6$).

the optical magnitude gap:

$$\Delta m_{12} = 2.5 \log_{10} \frac{(M_*)_1}{(M_*)_2}. \quad (5)$$

where $(M_*)_1$ is the stellar mass of the brightest member, and $(M_*)_2$ is the stellar mass of the second most massive galaxy in the group. We restrict the second most massive member to be within $0.5R_{\text{vir}}$. Since the most massive galaxies in groups are typically dominated by old stars, the stellar mass is expected to be a reasonable proxy for luminosity used observationally.

3. RESULTS

3.1. Overall Star Formation Histories

FGs and normal groups show very different star formation histories in our model, with the primary differentiator being a suppression in FGs of the overall group star formation rate at low redshift. Figure 4 shows the star formation histories of FGs and normal groups. We show the growth of stellar mass for the entire group (solid), and compare this to the stellar mass formed in-situ within the central galaxy (dashed). Both categories share a similar early history of star formation down to about $z \sim 3$, at which point their SFR start to deviate from one another. The SFR per unit redshift in FGs peak at a relatively high redshift, at $z \sim 2.5$, whereas SFR per unit redshift in normal groups continues to rise until peaking at $z \sim 1.7$. These trends in the SFR history of the central galaxies (dashed) follow that of the entire group for both cases. With respect to the overall amplitude of SFR, a significant difference between FGs and normal groups is seen: while in both cases the star formation histories of central galaxy and the entire group share a similar temporal shape and amplitude, the

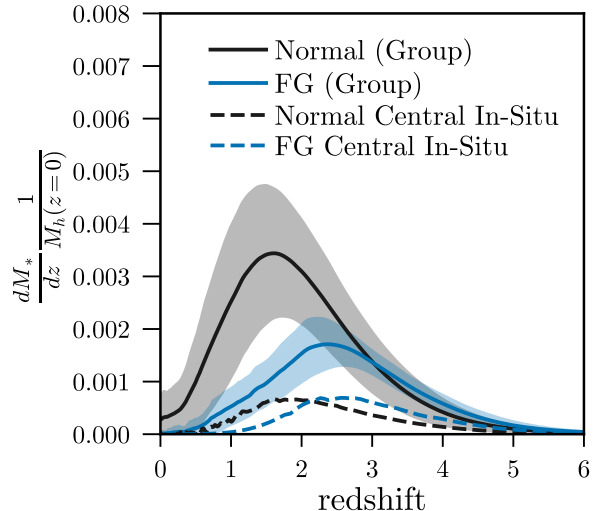


Figure 4. The formation rate of stellar mass per unit redshift as a function of redshift, dM_*/dz , divided by the final halo mass at $z = 0$, for the FGs (solid blue with shaded region) and normal (solid black with shaded region) samples with halo mass in the range of $10^{13.4} < M_h/M_\odot < 10^{13.6}$. We also show the same of the central galaxies for the two samples as dashed curves of matching colors. For each sample the shaded region represents the 1σ range.

mean ratio of star formation in the central vs. the group at the peak of group star formation is about 0.4 ± 0.1 in fossil groups, but 0.2 ± 0.1 in normal groups.

Consequently, the FG sample, on average, tends to harbor a central halo which is more massive in stellar mass than the normal groups at all redshifts. Since the star formation in FGs is considerably suppressed at the time of peak global star formation, the FGs tend to have lower stellar content. We now examine the underlying reasons for these differences between the two groups.

3.2. Shifted Self-Similar Halo Assembly Histories Between FGs and Normal Groups

The FGs have halo assembly histories which are shifted in time compared to the normal groups. Recall that we impose a transition halo mass M_c separating cold and hot accretion within our simplified star formation model. Figure 5 shows the median mass of the central halos of FGs (solid blue) and normal groups (solid black) as a function of redshift, along with a measure of the suppression of star formation at high halo mass in our model. We indicate the halo mass at which star formation is suppressed by a factor of two due to M_c . We see that the redshift at the crossing of the halo mass curves and M_c curve (orange horizontal dashed line) in Figure 5 is conformal, direction-wise, to the peak redshifts of star formation shown in Figure 4, for both FGs and normal groups. The FG and normal

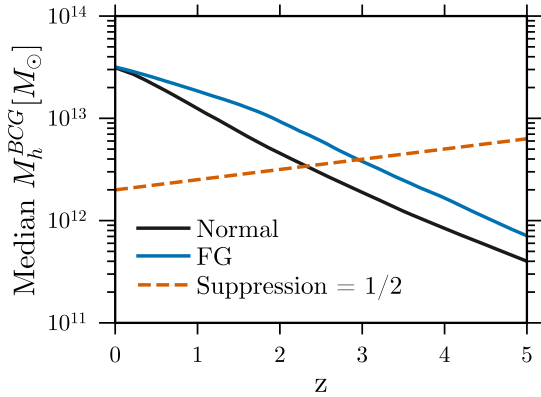


Figure 5. The median mass of the central halos of FGs (solid blue) and normal groups (solid black) as a function of redshift. Also shown as the dotted orange curve is the transition halo mass between cold and hot accretion such that star formation is suppressed by an 1/2.

groups cross the halo mass where star formation is suppressed by a factor of 2 at $z \sim 3$ for FGs versus $z \sim 2.3$ for normal groups. This is part of the cause for a similar difference in the redshift of peak star formation, which is $z \sim 2.5$ for FGs and $z \sim 1.7$ for normal groups. The lag between the redshift where substantial suppression starts and the peak redshift is because, while quenching occurs in the central halo, star formation may continue in satellites. We return to this point in 3.3.2. Overall, the assembly histories of FGs clearly differ from normal groups in terms of the assembly redshift, despite our selection for the same halo masses at $z = 0$.

The FGs also have satellite halos which follow their central halos in terms of earlier assembly histories. In the top panels of Figure 6 we show the redshift distribution of accreted halos in three different mass bins. We see that there is a clear shift to higher redshift (i.e., earlier accretion) for the most massive bins, $M_h = 10^{12} - 10^{12.5} M_\odot$, for FGs than normal groups, but the overall mass accreted in this halo mass bin is ultimately larger (by only $\sim 10\%$) for normal groups than for FGs. For the intermediate halo mass bin, $M_h = 10^{11} - 10^{12} M_\odot$, a similar shift is seen but the two groups accumulate to about the same amount by $z = 0$. Finally, for the lowest mass bin, $M_h = 10^{10} - 10^{11} M_\odot$, the shift is consistent and goes all the way to $z = 0$. This examination indicates that the earlier assembly of the the FG is shared by the satellite halos that are accreted by the respective main halos, over a large range of satellite masses. We shall call this phenomenon “halo assembly conformity”.

The conspicuous difference between the redshift and amplitude of SFR peaks between FGs and normal groups seen in Figure 4 raises the obvious question: do FGs and normal groups acquire halos subhalos in a

self-similar fashion with respect to the peak redshift? In other words, we ask whether the gravitational dynamics of FGs and normal groups are self-similar or not. To address this question, we track the number of subhalos accreted before and after the respective redshift of M_c crossing. In the top row of Figure 7 we show the histograms of the number of accreted satellite galaxies in three mass bins for FGs (blue curves) and normal groups (black curves) from high redshift down to the redshift for an individual group reaching M_c . The bottom row of Figure 7 is similar to the top row but for the redshift range of $z = 0$ to $z = z_{peak}$.

In both redshift ranges, demarcated by the respective redshift peak, no statistically significant differences are seen between FGs and normal groups with respect to the mass distribution of satellite halos. From this we can conclude that the gravitational dynamics alone, i.e., the number of halos or the type of halos accreted, is not a direct cause for the difference in the amplitude and redshift of the star formation peak between FGs and normal groups, if the stellar content of a galaxy depends only on the halo mass. Thus, the difference in stellar masses between FGs and normal groups ought to be rooted in the difference in stellar mass to halo mass ratios between those comprising FGs and those comprising normal groups.

3.3. Origin of Stellar Content Difference between FGs and Normal Groups

3.3.1. Baryonic Environment Effects

We argue that quenching effects coming from the environments of satellites do not play a major role in the stellar content differences between FGs and normal groups. FGs and normal groups both experience some degree of environmental quenching in our model, when the central halo mass grows more massive than M_c and enters the hot accretion regime. We apply to the bound subhalos the same suppression factor that the more massive central halo experiences, to model an environmental suppression by the central halo on star formation in the satellites. We impose this same suppression factor on every satellite halo within three virial radii based on hydrodynamic simulations (Cen 2014). Since the central halos of FGs become more massive at earlier times, the difference in stellar content for FGs and normal groups at $z = 0$ is then a result of both satellites and central progenitors of FGs have lower stellar content than their counterparts of normal groups. We argue in this section that these effects are subdominant, by comparing the stellar content of the same groups, using models with and without this effect.

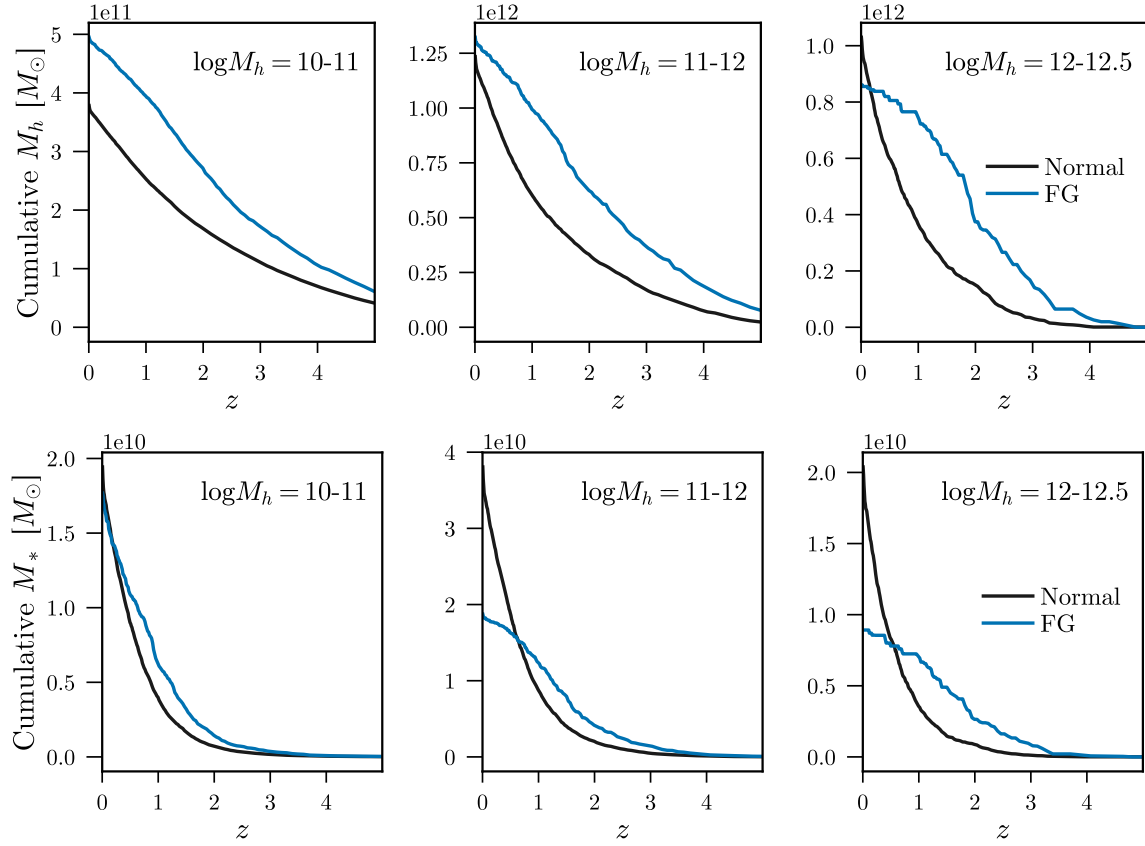


Figure 6. The top row shows the cumulative dark matter mass from mergers onto the progenitor, of halos in three different mass bins, $\log M_h/M_\odot = 10 - 11$ (left panel), $\log M_h/M_\odot = 11 - 12$ (middle panel) and $\log M_h/M_\odot = 12 - 12.5$ (right panel), for FGs (blue dashed curves) and normal groups (black solid curves), respectively. The bottom row shows the corresponding cumulative stellar mass.

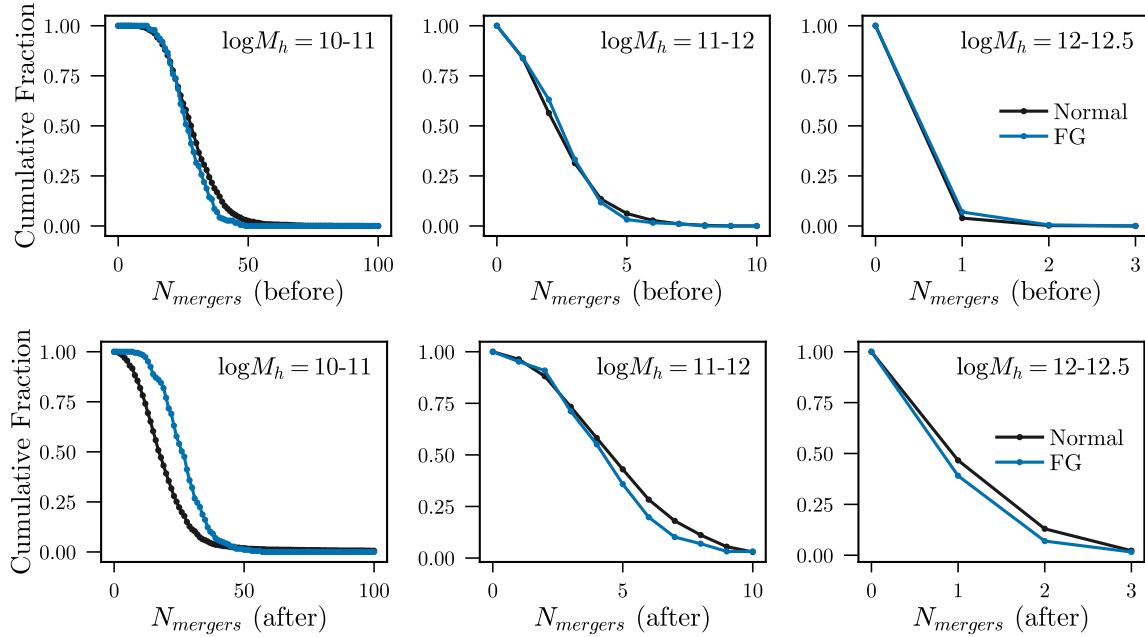


Figure 7. Cumulative merger counts before first crossing M_c for normal and FG.

Type	$z_{1/2}$	$z_{1/2}$
	merged	$z = 0$ sat
FG (env)	1.1	1.7
FG (no env)	0.9	1.4
Normal (env)	0.45	0.63
Normal (no env)	0.43	0.65

Table 1. The effects of environmental suppression on mass evolution with redshift. We show stellar mass in progenitors which have already merged into the central (“merged”) and stellar mass in progenitors of present-day group members which have not yet merged (“ $z = 0$ sat”).

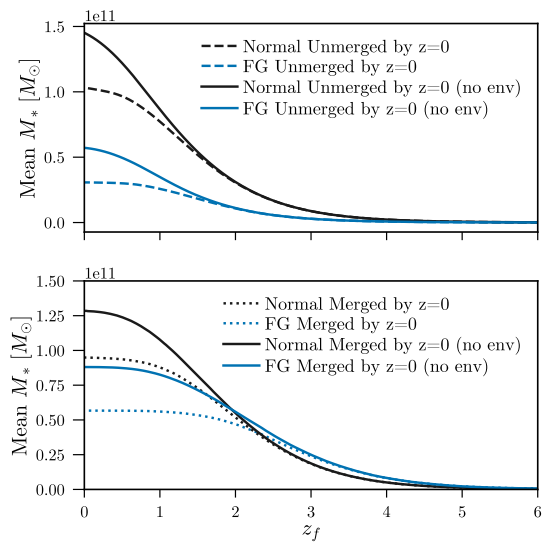


Figure 8. We show the effect of the environmental suppression for both normal and FG. Summary statistics like the half-mass redshift are provided in Table 1. In the top panel, we show stellar mass in progenitors of present-day group members which have not yet merged. We show these for normal groups (black) and FG (blue), with environmental suppression (dashed) and without (solid). In the lower panel, we show the same quantities for progenitors of the central halo which have already merged by redshift 0.

We show in Figure 8 that the environment effect is significant but is unable to account for most of the difference in the stellar content between FGs and normal groups. The top panel of the figure shows the growth of stellar mass in progenitors of present-day group members which have not yet merged with the central halo. In both normal groups and FGs, the environmental suppression has a $\sim 20\%$ impact on the final stellar mass. A similar magnitude is shown in the bottom panel, which shows the mass growth of stellar mass in progenitors which have already merged at $z \sim 0$. The normal groups

and FGs both experience a similar amount of lost final stellar mass from mergers. This indicates that environment effect is significant but does not constitute a major contributor to the difference of stellar content at $z = 0$ between FGs and normal groups. But this findings is in apparent contradiction to the redshift evolution of stellar mass shown in Figures 4, 6 and in Figure 10 below. We continue looking for the main culprit and a self-consistent physical explanation.

3.3.2. Effects due to Central-Satellite Halo Assembly Conformity

The earlier assembly of main halos for FGs is paralleled, in time, by a corresponding stellar component in an increasingly amplified way with increasing subhalo masses. In the bottom row of Figure 6 we show the redshift distribution of accreted stellar mass from the halos for three different mass bins. A differential behavior for halos with different masses is visible: the ratio of the cumulative stellar mass of FGs to that of normal groups is seen to increase with increasing halo mass of the subhalo. This suggests decreased star formation rates in subhalos of higher masses of FGs relative to their counterparts of normal groups. In other words, while stars in FGs form earlier and at a lower efficiency than their counterparts in normal groups, the difference increases with the halo mass of subhalos.

Figure 9 shows the redshift evolution of the stellar-mass-to-halo-mass ratio for halos in three $\log_{10} M_h$ ranges in three separate panels. A similar difference is seen for halos of mass in the range $10^{11} - 10^{12} M_\odot$ (middle panel) and $10^{10} - 10^{11} M_\odot$ (left panel), except that for the smallest halo mass bin the distributions at all redshifts peak close to zero, suggesting a large number of starless subhalos. In all cases, the trend of increasing stellar to halo mass ratio with decreasing redshift continue to $z = 0$ (solid curves in all panels). Thus, Figure 9 may be able to provide the reason why FGs are more stellar deficient than the normal groups, simply because progenitors of FGs mature (i.e., crossing M_c) at a higher redshift than the normal groups, when the stellar to halo mass ratio of all constituents accreted is generally lower by a factor of roughly two. Observationally, it is found that high redshift galaxies are indeed more gas rich and relatively stellar poor at a given halo mass of relevance (e.g., Carilli & Walter 2013), consistent with our model results.

We argue that another part of the lower stellar content in fossil groups comes from this global relationship between redshift and richness demonstrated in Figure 9, combined with the earlier satellite accretion histories of FGs compared to normal groups. The stellar-mass-to-halo-mass ratio shown in Figure 9 is the ratio at the

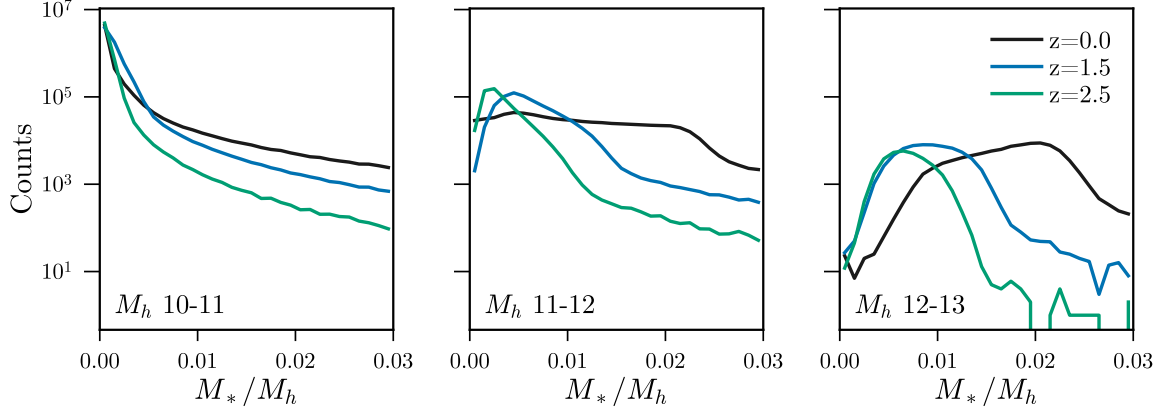


Figure 9. The redshift evolution of the stellar-mass-to-halo-mass ratio for halos of $\log_{10} M_h = 10 - 11$ (left), $11 - 12$ (middle) and $12 - 12.5$ (right). In general, high redshift halos tend to be deficient in stellar mass. The global stellar-mass-to-halo-mass ratio evolves from 0.005 to 0.01 and then 0.02 at $z = 2.5, 1.5$ and 0.0 , respectively, shown.

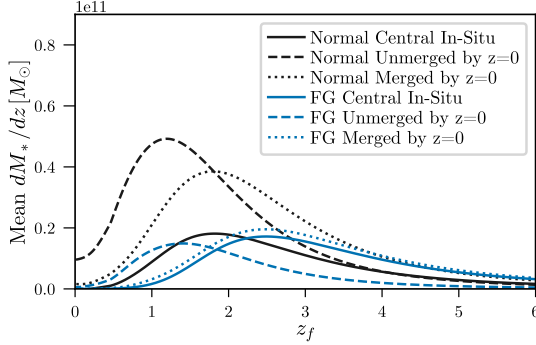


Figure 10. The stellar mass as a function of the **formation** redshift for three separate components: in-situ star formation in the main progenitor (solid curve), accreted satellites that have merged into the central BCG (dotted curve) and accreted satellites that have not merged into the central BCG (i.e., satellites of the BCG at $z = 0$, dashed curve), for FGs (blue curves) and normal groups (black curves), respectively.

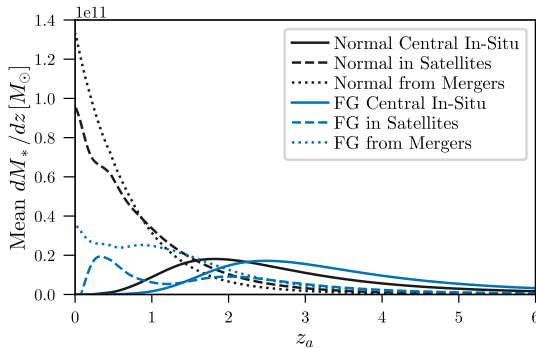


Figure 11. The stellar mass as a function of the **accretion** redshift for three separate components: in-situ star formation in the main progenitor (solid curve), accreted satellites that have merged into the central BCG (dotted curve) and accreted satellites that have not merged into the central BCG (i.e., satellites of the BCG at $z = 0$, dashed curve), for FGs (blue curves) and normal groups (black curves), respectively.

respective redshift, which may be different from the ratio at the time of accretion/acquisition by the central galaxies. To check this, Figure 10 shows the stellar mass accumulated as a function of the star formation redshift classified into three types: in-situ star formation in the main progenitor (solid curve), accreted from satellites that have merged into the central BCG by $z = 0$ (dotted curve) and accreted from satellites that have not merged into the central BCG by $z = 0$ (i.e., satellites of the BCG at $z = 0$, dashed curve), separately for FGs (blue curves) and normal groups (black curves).

The star formation histories of both in-situ stars and ex-situ stars of normal groups may be approximately obtained by shifting the peaks of their counterparts of FGs to lower redshifts by roughly $\Delta z \sim (1.2, 0.7, 0.1)$ for (in-situ, ex-situ merged, ex-situ unmerged), respectively. In terms of star formation age, the three components in the order of increasing age are (in-situ, ex-situ merged, ex-situ unmerged) for the FGs, with the “in-situ” component being older than the “ex-situ merged” only by about $\Delta z \sim 0.5$. The “ex-situ merged” component is older than the “ex-situ unmerged” component by $\Delta z \sim 1$ for FGs. The situation for normal groups display quite different behaviors. We see that the in-situ stars in normal groups are on average slightly younger than the accreted merged stars but older than the accreted unmerged stars. Consequently, in the BCGs of FGs there is an old-to-young stellar age gradient from the center to the outskirts, where the opposite is expected for normal groups. Moreover, the age contrast between central BCGs and satellite galaxies in BCGs is expected to be much larger than that for normal groups. These predictions are important and should be testable observationally.

We find that the fossil groups have very different satellite histories. Figure 11 shows the stellar mass as a func-

tion of the **accretion** redshift for three separate components: in-situ star formation in the main progenitor (solid curve), accreted satellites that have merged into the central BCG (dotted curve) and accreted satellites that have not merged into the central BCG (i.e., satellites of the BCG at $z = 0$, dashed curve), for FGs (blue curves) and normal groups (black curves), respectively. The histories of the in-situ star formation rate, as a function of formation redshift in Figure 10, identical to that as a function of accretion redshift in Figure 11, for FGs and normal groups, display similar shapes characterized by a gradual rise at early times ($z > 2.5$) followed by a somewhat steeper decline past the peak towards lower redshift ($z < 2.5$). The location of the in-situ star formation peak coincides with the time when the central halo of the group enters hot accretion mode, with FGs peaking at $z \sim 2.5$ compared to a peak at $z \sim 2$ for normal groups.

However, a comparison of dashed curves (unmerged satellites) or dotted curves (merged satellites) between Figure 11 and Figure 10 indicates that the formation redshift and accretion redshift of stars in satellites are very different. In particular, while the formation redshift of satellites display a shape - early rise followed by late decline - similar to that of the in-situ star formation, albeit with different peak locations, the accretion redshift of stars in satellites have different, varied temporal profiles. Third, perhaps profoundly, the difference in accretion redshift distribution between FG satellites and normal group satellites is large. We see that, whereas the accretion rates of both merged and unmerged satellites in normal groups' satellites continue to rise until $z = 0$, the accretion rate of merged satellites of FGs initially rise from $z \sim 2$ to $z \sim 1$ and then largely flat, only to be followed by a moderate rise from $z \sim 0.2$ to $z = 0$, and the accretion rate of unmerged satellites of FGs shows a very gradual rise from high redshift to $z \sim 2$ then declines to $z \sim 1.3$, followed by a rise to $z \sim 0.3$, after which it declines until $z = 0$. We have yet to fully understand the physical reasons behind the complexity of this behavior.

To summarize the complex trends in simple terms: (1) The central galaxies and satellite galaxies in FGs formed relatively earlier than their counterparts in normal groups. (2) There is a general trend of decreasing stellar mass to halo mass ratio with increasing redshift at a given halo mass. (3) The satellite galaxies in FGs get acquired by their central galaxies at higher redshifts than their counterparts in normal groups. (4) There is varying redshift intervals between the stellar assembly redshift and accretion redshift of satellite galaxies in both FGs and normal groups. Altogether, the differen-

Model	$M_*^{\text{FG}}(z=0)$ [$10^{11}M_\odot$]	$M_*^{\text{normal}}(z=0)$ [$10^{11}M_\odot$]
env	1.4	2.4
no env	1.9	3.1

Table 2. The effects of environmental suppression on total group stellar mass at $z = 0$. The star formation suppression in FGs arises $\sim 70\%$ from gravitational effects (the difference in the bottom row of this table) and $\sim 30\%$ from environmental effects (the difference in the left column).

Model	$M_*^{\text{FG}}/M_*^{\text{normal}}$ merged	$M_*^{\text{FG}}/M_*^{\text{normal}}$ $z = 0$ sat
env	0.61	0.37
no env	0.70	0.49

Table 3. The effects of environmental suppression on relative stellar mass deficiency in our fossil groups, from different mass sources. The "merged" column refers to stellar mass in the central, obtained only from mergers. The $z = 0$ sat column refers to mass in satellites in the group at $z = 0$.

tial between formation and accretion redshifts and the differential of those between FGs and normal groups ultimately contribute to the about 70% of the difference in stellar content between FGs and normal groups at $z = 0$, whereas baryonic environmental effects account for about 30% of the difference.

Since the amount of dark matter mass in FG halos and normal groups is the same and since the number and mass distribution of halos accreted before and after the central halo assembly redshift are the same for FGs and normal groups (see Figure 7), whatever physical effects responsible for the difference in stellar content between FGs and normal groups must be then pertaining to baryonic effects that affect star formation. We ultimately ascribe the effect to declining star formation efficiency with decreasing redshift from roughly at the peak to $z = 0$ reflected in the temporal shape of the Madau plot (i.e. the right panel of Figure 1). Note that the Madau plot shows instantaneous star formation with respect to redshift, rather than time. Thus the peak of the Madau plot does not exactly correspond to either when the majority of star formation occurs, nor the time of peak star formation efficiency. Thus, the Madau plot is in fact consistent with both an increasing star formation rate and a decreasing stellar mass to halo mass halo with increasing redshift at a given halo mass.

Our model predicts that the stellar mass within the "unmerged" satellite component should display a rapid

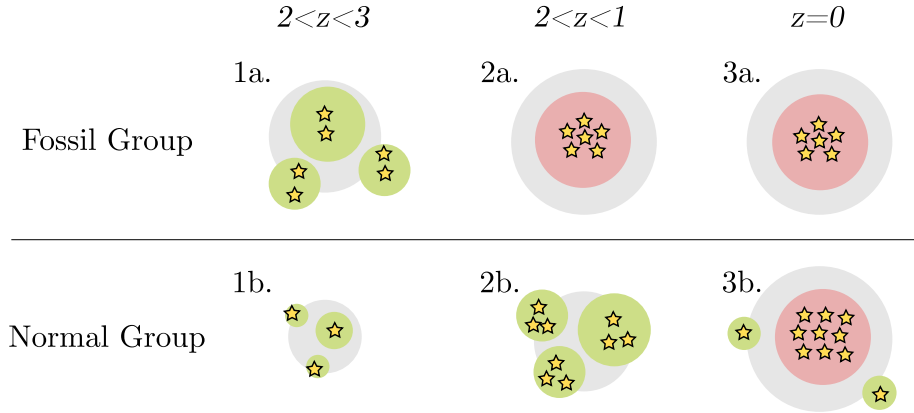


Figure 12. A visual illustration of the essence of the key trend our model predicts. The top and bottom rows are the star formation and halo growth history for FGs and typical groups of the same mass at $z = 0$, respectively. In a typical group (the bottom row), star-forming galaxies (green) begin to cluster at redshift ~ 3 (1a). They continue to accrete matter and form stars (1b) at redshifts $2 < z < 1$, until hierarchical merging leads to a local gravitational potential which heats the gas enough to quench star formation (1c). Our FGs also begin as star-forming galaxies at high redshift (2a), but assemble their halos earlier. Our FGs come from more concentrated initial density fluctuations, leading to a more massive central progenitor at redshift ~ 2 (2b). This quenches star formation early in the central halo, but also suppresses star formation in satellites within a few virial radii (shown as a dashed line). Star-forming galaxies in our model FGs tend to be consumed by the central halo earlier than in typical groups (2a to 2b), and such high-redshift galaxies tend to have lower stellar mass at fixed halo mass. The surviving satellites (2b) are quenched by heating of the environment by the central halo. The end result (2c) is a group-sized halo with the same halo mass, but has lower stellar mass.

drop from $z \sim 0.3$ to $z = 0$ in FGs, where this component in normal groups continues to rise rapidly towards $z = 0$. Thus, our model says that the radial distribution of satellite galaxies in normal groups is significantly more extended than that of the FGs. This also manifests in the difference in galaxy correlation functions shown later. Another possible testable prediction is also noted. While the “merged” satellite component is older than the “unmerged” satellite component in FGs, the former is accreted later than the latter to their respective locations. This last point may be indicative that while there is continued merging of satellites into the central BCGs of FGs, the supply rate of satellites into the FGs (through the virial radii) is much lower at low redshift.

We now summarize the physical picture that has emerged from our analysis in a cartoon, shown in Figure 12. We see that the FG halos assemble earlier than normal groups, as indicated by the larger satellite halos with more stars in the top left panel compared to the bottom left panel at $z \sim 2 - 3$. By $z = 1 - 2$ the FGs have largely matured, whereas the normal groups now just entered their prime star formation and halo/stellar accretion peak, as indicated by the middle panels. The most important point to notice is that the satellite halos of a same mass that is accreted by normal groups at $z = 1 - 2$ are more stellar rich than those accreted by FGs at $z = 2 - 3$. By $z = 0$, the cumulative difference

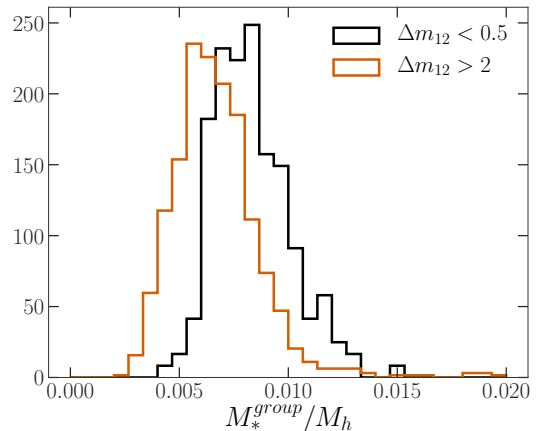


Figure 13. Two separate probability distribution function of stellar to halo ratios of groups shown in Figure (2), by subdividing the groups according to the optical magnitude gap between the brightest and second brightest galaxy in each group, Δm_{12} . Each distribution is normalized to yield the integral to be unity.

in stellar mass accreted from satellites and in-situ star formation result in the difference in stellar mass between FGs and normal groups.

3.4. Comparison with Magnitude Gap Methods

We have selected FGs based on stellar mass deficiency, which we argue is less susceptible to the randomness associated with observing the $z \sim 0$ snapshot of structure

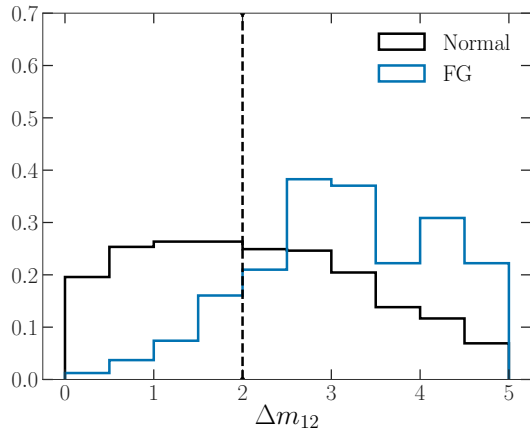


Figure 14. Normalized histograms of magnitude gap in the normal and FG samples, with the traditional criteria of Δm_{12} approximated by the dotted line.

formation. This method corresponds to a stellar to halo mass ratio of 0.005 for groups of halo masses in the range $10^{13.4} < M_h/M_\odot < 10^{13.6}$, with the remaining, stellar rich halos being the normal sample. Now in Figure (13) we show the distribution of the optical magnitude gap between the brightest and second brightest galaxy in each group for the FGs and the normal sample. We see that FGs tend to exhibit larger magnitude gaps than normal groups. This indicates that this frequently used selection method based on optical magnitude gap, while not the most stable in the context of hierarchical growth model due to random merger timing, does show a tendency in the right sense in that the stellar deficient FGs, as a whole, have a larger Δm_{12} than the normal groups. In other words, there is indeed a broad correlation between stellar deficiency and Δm_{12} . However, the difference in the stellar mass to halo mass ratio between the two samples based on Δm_{12} is rather small and there is a large overlap between the two distributions. This makes Δm_{12} is less sensitive parameter to untangle the stellar growth history of groups.

Figure 14 shows the distributions of Δm_{12} for the FGs and normal groups. Here we see that the gap Δm_{12} for FGs tends to be much larger than those of normal groups, with a typical FG selected through stellar deficiency having a magnitude gap of ~ 3 , compared to the broad distribution peaking at $\Delta m_{12} \sim 1.5$ for gaps in the normal population. The comparison between Figure (13) and Figure (14) is very interesting and perhaps shows more clearly the pros and cons of the selection methods. The Δm_{12} based method suggests that the groups with the largest gaps ($\Delta m_{12} > 2$) tend to have 20% lower M_*^{group}/M_h , resulting in about $\sim 20\%$ of the large gap ($\Delta m_{12} > 2$) groups fulfilling our stellar de-

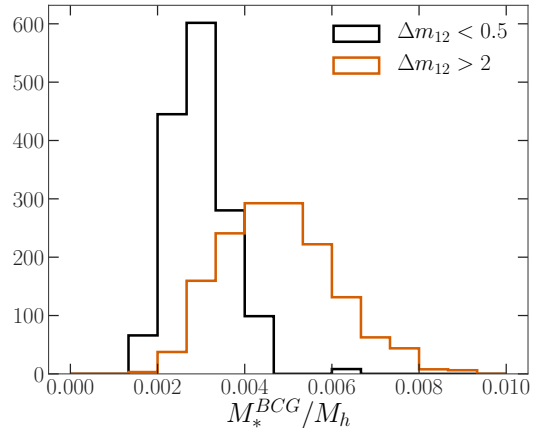


Figure 15. (updated figure) shows the distributions of stellar mass to halo mass ratios based on Δm_{12} selection. Selecting on magnitude gap does yield a sample with a higher BCG stellar mass.

ficiency criteria of $M_*^{\text{group}}/M_h > 0.005$. In contrast, our stellar deficiency our stellar content based selection method does produce a more pronounced differentiation in Δm_{12} between the two types of groups.

Despite a simple selection method, our results based on Δm_{12} are in fact consistent with recent observations (Voevodkin et al. 2010; Harrison et al. 2012; Kundert et al. 2015), which suggest that optical and X-ray luminosity of $\Delta m_{12} > 2$ selected fossil groups are similar to those of typical groups, since the difference in the mean M_*^{group}/M_h is a small fraction of the intrinsic scatter in the population, as we show. It may be that historically small samples from the large magnitude gap population may have by chance exhibited a stronger difference in mass to light ratios, but larger sample sizes from more recent surveys have better probed the intrinsic scatter, resulting in two samples which are statistically consistent to within current observational limits.

3.5. On Significant Difference in BCGs between FGs and Normal Groups

So far our pair-wise comparisons between FGs and normal groups are focused on the entire group. We now turn to the brightest central galaxies in the groups. Given the existing literature on selecting FGs based on magnitude gap, we first show in Figure 15 the distributions of bright central galaxy stellar mass to total stellar mass ratio based on Δm_{12} selection. Interestingly, an opposite trend is seen here: groups with larger magnitude gaps tend to have brighter BCGs, versus the trend seen in Figure (13) where groups with larger magnitude gaps tend to have lower total stellar masses. Quite encouragingly, this result is consistent with observations involving the usual gap selection criteria for FGs (Har-

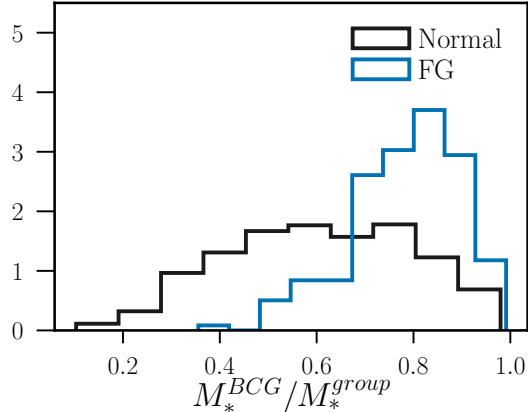


Figure 16. The ratio of stellar mass in BCG over the total stellar mass in the groups, for FGs (blue curve) and normal groups (black curve). These groups have been selected in the narrow halo mass range $10^{13.4}M_{\odot} < M_h < 10^{13.6}$ to control for other forms of halo bias. The union of these two populations forms the full halo population in this range.

risson et al. 2012), providing a connection between the magnitude-gap selected "fossil groups" and the groups we define as FGs.

In Figure 16 we show the ratio of stellar mass in BCG over the total stellar mass in the groups, for FGs (blue curve) and normal groups (black curve). Thus, we predict that FGs have brighter BCGs compared to normal groups. This prediction should be testable as well.

3.6. Significant Difference in Spatial Clustering between FGs and Normal Groups

One can test our model through the galaxy-group cross-correlation between the FGs and normal group. We show in top and bottom panels of Figure 17 the predicted cross-correlation functions between groups and two sets of satellite galaxies respectively: relatively massive galaxies ($M_h > 10^{12} M_{\odot}$) and less massive galaxies ($M_h < 10^{11} M_{\odot}$). We see that, in both cases, galaxies are less strongly clustered with FGs than with normal groups on scales less than about 1 Mpc/h, while on larger scales the difference is very small. Moreover, the difference on $< 1\text{Mpc}$ is larger for more massive satellite galaxies than for less massive satellite galaxies. Since the scale $\sim 1\text{Mpc}$ is roughly about the virial radius of the groups in question, we might summarize the above results in a more succinct way. This is consistent with the fact that FGs form early that will be shown later. More specifically, this is in excellent agreement with the trend seen in Figure 11, showing that, while there is continued merging of satellites into the central BCGs of FGs, the supply of satellites into the FGs (through the

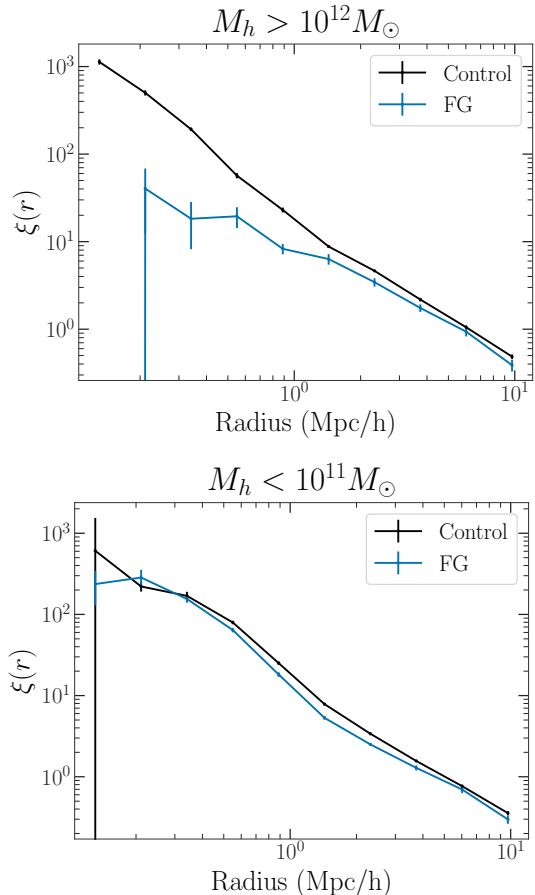


Figure 17. Top panel shows the cross correlation function between massive halos ($M_h > 10^{12} M_{\odot}$) and [FG (blue solid curve), normal groups], respectively. FG halos tend to have fewer massive neighbors within 1 Mpc/h. Bottom panel shows the cross correlation function between less massive halos ($M_h = 10^{11} - 10^{12} M_{\odot}$) and [FG (blue solid curve), normal groups], respectively, where FGs shows only a slight deficiency in such halos within about 1Mpc/h. Error bars were performed with a jackknife using `halotools` (Hearin et al. 2017).

virial radii) is much lower at low redshift compared to that of normal groups.

4. CONCLUSION

We performed detailed modeling and analysis to produce a physical picture connecting the assembly history and stellar deficiency of fossil groups (FGs). Fossil groups are typically We normalize our model parameters to match the observed galaxy stellar function mass function at $z = 0$ and the observed star formation rate density evolution (the Madau plot). We reach the following conclusions and predictions.

1. Fossil groups assemble earlier than normal groups, redshift $z \sim 2.5$ versus $z \sim 1.5$, hence the name

- “fossil”. In-situ star formation terminates earlier in fossil groups than normal groups. Stellar mass formed in satellite halos that are ultimately accreted to reside within the virial radius of the group displays a roughly conformal behavior to the central progenitor with respect to star formation efficiency in both cases. Halos accreted by fossil groups form earlier than those accreted by normal groups. There is thus a twin-conformity between central galaxies and satellites between FGs and normal groups: centrals and satellites in the former form earlier and more stellar deficient than their counterparts of the latter. We term this effect “assembly conformity” of halos. This effect accounts for about 70% of the difference in stellar content between FGs and normal groups. This is relevant to observations focused on the magnitude gap, such as [Trevisan et al. 2017](#), [Raouf et al. 2019](#), which have suggested that large gap systems have more mergers to the central, but at higher redshift to cause no detectable imprints in SFH.
2. If one “stacks” merger histories centered on the redshift of the peak star formation rate per unit redshift, we find that the mass functions of satellite halos on either side of the peak redshift are indistinguishable between FGs and normal groups, indicating a self-similarity of halo assembly with respect to the peak. Thus, the “assembly conformity” of halos above is ultimately a baryonic effect related to star formation efficiency but seeded by the timing of formation of centrals and satellites, not their halo masses.
 3. Once the central galaxies enter the hot accretion mode, it also exerts “baryonic environmental” effects in the form of ram-pressure removal of cold gas in satellite galaxies and heating of gas to high temperature to prevent accretion of ample cold gas to satellite galaxies. This effect account for about 30% of the difference in stellar content between FGs and normal groups.
 4. In both fossil and normal groups, the formation redshift of stars in subhalos is higher than the accretion redshift, with the difference larger for fossil groups. Generally, at any given halo mass, galaxies have increasingly higher stellar to halo mass ratio with decreasing redshift.
 5. While the total stellar mass of FGs is lower than that of normal groups, we find that the mass of the brightest central galaxy is, on average, higher

than that of normal groups. This prediction is verifiable.

6. We predict that in the central galaxies of FGs, there is a negative stellar age gradient from the center outward, where the opposite is expected for those in normal groups. Moreover, the age contrast between central and satellite galaxies in FGs is expected to be much larger than that for normal groups. These unique predictions are important and should be testable observationally.
7. Finally, we find that the cross-correlation function between Milky-size satellite halos and FGs is weaker than that between such satellites and normal groups by at a factor of a few at a separation of 0.5Mpc (and still larger at smaller separations). This may be observationally verifiable as well.

We thank Dr. Jia Liu for kindly providing references for the observational data used for the right panle of Figure 1. We thank Anatoly Klypin for Bolshoi simulations that are used in our analysis. The research is supported in part by NASA grant 80NSSC18K1101.

APPENDIX

REFERENCES

- Adami, C., Jouvel, S., Guennou, L., et al. 2012, *A&A*, 540, A105
- Bahé, Y. M., McCarthy, I. G., Balogh, M. L., & Font, A. S. 2013, *MNRAS*, 430, 3017
- Balogh, M. L., Morris, S. L., Yee, H. K. C., Carlberg, R. G., & Ellingson, E. 1999, *ApJ*, 527, 54
- Barnes, J. E. 1989, *Nature*, 338, 123
- Benson, A. J. 2012, *NewA*, 17, 175
- Bharadwaj, V., Reiprich, T. H., Sanders, J. S., & Schellenberger, G. 2016, *A&A*, 585, A125
- Bouwens, R. J., Illingworth, G. D., Oesch, P. A., et al. 2012a, *ApJL*, 752, L5
- . 2012b, *ApJ*, 754, 83
- Bower, R. G., Benson, A. J., Malbon, R., et al. 2006, *MNRAS*, 370, 645
- Carilli, C. L., & Walter, F. 2013, *ARA&A*, 51, 105
- Cen, R. 2014, *ApJ*, 789, L21
- Crain, R. A., Theuns, T., Dalla Vecchia, C., et al. 2009, *MNRAS*, 399, 1773
- Cucciati, O., Tresse, L., Ilbert, O., et al. 2012, *A&A*, 539, A31
- Cui, W., Springel, V., Yang, X., De Lucia, G., & Borgani, S. 2011, *MNRAS*, 416, 2997
- Dahlen, T., Mobasher, B., Dickinson, M., et al. 2007, *ApJ*, 654, 172
- Dariush, A., Khosroshahi, H. G., Ponman, T. J., et al. 2007, *MNRAS*, 382, 433
- Dariush, A. A., Raychaudhury, S., Ponman, T. J., et al. 2010, *MNRAS*, 405, 1873
- Díaz-Giménez, E., Zandivarez, A., Proctor, R., Mendes de Oliveira, C., & Abramo, L. R. 2011, *A&A*, 527, A129
- D’Onghia, E., Sommer-Larsen, J., Romeo, A. D., et al. 2005, *ApJ*, 630, L109
- Dunne, L., Ivison, R. J., Maddox, S., et al. 2009, *MNRAS*, 394, 3
- Eigenthaler, P., & Zeilinger, W. W. 2013, *A&A*, 553, A99
- Gozaliasl, G., Khosroshahi, H. G., Dariush, A. A., et al. 2014, *A&A*, 571, A49
- Grupponi, C., Pozzi, F., Rodighiero, G., et al. 2013, *MNRAS*, 432, 23
- Haines, C. P., Pereira, M. J., Smith, G. P., et al. 2015, *ApJ*, 806, 101
- Harrison, C. D., Miller, C. J., Richards, J. W., et al. 2012, *ApJ*, 752, 12
- Hearin, A. P., Behroozi, P. S., & van den Bosch, F. C. 2016, *MNRAS*, 461, 2135
- Hearin, A. P., Campbell, D., Tollerud, E., et al. 2017, *AJ*, 154, 190
- Henriques, B. M. B., White, S. D. M., Thomas, P. A., et al. 2015, *MNRAS*, 451, 2663
- Jones, L. R., Ponman, T. J., Horton, A., et al. 2003, *MNRAS*, 343, 627
- Kajisawa, M., Ichikawa, T., Yamada, T., et al. 2010, *ApJ*, 723, 129
- Kanagusuku, M. J., Díaz-Giménez, E., & Zandivarez, A. 2016, *A&A*, 586, A40
- Karim, A., Schinnerer, E., Martínez-Sansigre, A., et al. 2011, *ApJ*, 730, 61
- Katz, N. 1992, *ApJ*, 391, 502
- Kauffmann, G., White, S. D. M., & Guiderdoni, B. 1993, *MNRAS*, 264, 201
- Kereš, D., Katz, N., Fardal, M., Davé, R., & Weinberg, D. H. 2009, *MNRAS*, 395, 160
- Khosroshahi, H. G., Gozaliasl, G., Rasmussen, J., et al. 2014, *MNRAS*, 443, 318
- Khosroshahi, H. G., Ponman, T. J., & Jones, L. R. 2007, *MNRAS*, 377, 595
- Khosroshahi, H. G., Raouf, M., Miraghaei, H., et al. 2017, *ApJ*, 842, 81
- Klypin, A., Yepes, G., Gottlöber, S., Prada, F., & Heß, S. 2016, *MNRAS*, 457, 4340
- Klypin, A. A., Trujillo-Gomez, S., & Primack, J. 2011, *ApJ*, 740, 102
- Krick, J. E., & Bernstein, R. A. 2007, *AJ*, 134, 466
- Kundert, A., D’Onghia, E., & Aguerra, J. A. L. 2017, *ApJ*, 845, 45
- Kundert, A., Gastaldello, F., D’Onghia, E., et al. 2015, *MNRAS*, 454, 161
- La Barbera, F., de Carvalho, R. R., de la Rosa, I. G., et al. 2009, *AJ*, 137, 3942
- Le Borgne, D., Elbaz, D., Ocvirk, P., & Pichon, C. 2009, *A&A*, 504, 727
- Ly, C., Lee, J. C., Dale, D. A., et al. 2011a, *ApJ*, 726, 109
- Ly, C., Malkan, M. A., Hayashi, M., et al. 2011b, *ApJ*, 735, 91
- Magnelli, B., Elbaz, D., Chary, R. R., et al. 2011, *A&A*, 528, A35
- Magnelli, B., Popesso, P., Berta, S., et al. 2013, *A&A*, 553, A132

- Miller, E. D., Rykoff, E. S., Dupke, R. A., et al. 2012, *ApJ*, 747, 94
- Moustakas, J., Coil, A. L., Aird, J., et al. 2013, *ApJ*, 767, 50
- Pierini, D., Giodini, S., Finoguenov, A., et al. 2011, *MNRAS*, 417, 2927
- Pillepich, A., Springel, V., Nelson, D., et al. 2018, *MNRAS*, 473, 4077
- Planck Collaboration, Ade, P. A. R., Aghanim, N., et al. 2014, *A&A*, 571, A16
- Proctor, R. N., de Oliveira, C. M., Dupke, R., et al. 2011, *MNRAS*, 418, 2054
- Proctor, R. N., Mendes de Oliveira, C., & Eigenthaler, P. 2014, *MNRAS*, 439, 2281
- Raouf, M., Khosroshahi, H. G., Mamon, G. A., et al. 2018, *ApJ*, 863, 40
- Raouf, M., Khosroshahi, H. G., Ponman, T. J., et al. 2014, *MNRAS*, 442, 1578
- Raouf, M., Shabala, S. S., Croton, D. J., Khosroshahi, H. G., & Bernyk, M. 2017, *MNRAS*, 471, 658
- Raouf, M., Smith, R., Khosroshahi, H. G., et al. 2019, *ApJ*, 887, 264
- Reddy, N. A., & Steidel, C. C. 2009, *ApJ*, 692, 778
- Robotham, A. S. G., & Driver, S. P. 2011, *MNRAS*, 413, 2570
- Rujopakarn, W., Eisenstein, D. J., Rieke, G. H., et al. 2010, *ApJ*, 718, 1171
- Salim, S., Rich, R. M., Charlot, S., et al. 2007, *ApJS*, 173, 267
- Sanders, D. B., Mazzeella, J. M., Kim, D.-C., Surace, J. A., & Soifer, B. T. 2003, *AJ*, 126, 1607
- Schaye, J., Dalla Vecchia, C., Booth, C. M., et al. 2010, *MNRAS*, 402, 1536
- Schenker, M. A., Robertson, B. E., Ellis, R. S., et al. 2013, *ApJ*, 768, 196
- Schiminovich, D., Ilbert, O., Arnouts, S., et al. 2005, *ApJL*, 619, L47
- Shim, H., Colbert, J., Teplitz, H., et al. 2009, *ApJ*, 696, 785
- Smolčić, V., Schinnerer, E., Zamorani, G., et al. 2009, *ApJ*, 690, 610
- Sobral, D., Smail, I., Best, P. N., et al. 2013, *MNRAS*, 428, 1128
- Somerville, R. S., & Primack, J. R. 1999, *MNRAS*, 310, 1087
- Springel, V. 2005, *MNRAS*, 364, 1105
- Tadaki, K.-I., Kodama, T., Koyama, Y., et al. 2011, *PASJ*, 63, 437
- Takeuchi, T. T., Yoshikawa, K., & Ishii, T. T. 2003, *ApJL*, 587, L89
- Trevisan, M., Mamon, G. A., & Khosroshahi, H. G. 2017, *MNRAS*, 464, 4593
- Trujillo-Gomez, S., Klypin, A., Primack, J., & Romanowsky, A. J. 2011, *ApJ*, 742, 16
- van der Burg, R. F. J., Hildebrandt, H., & Erben, T. 2010, *A&A*, 523, A74
- Vikhlinin, A., McNamara, B. R., Hornstrup, A., et al. 1999, *ApJ*, 520, L1
- Voevodkin, A., Borozdin, K., Heitmann, K., et al. 2010, *ApJ*, 708, 1376
- Vogelsberger, M., Marinacci, F., Torrey, P., & Puchwein, E. 2020, *Nature Reviews Physics*, 2, 42
- Vogelsberger, M., Genel, S., Springel, V., et al. 2014, *MNRAS*, 444, 1518
- von Benda-Beckmann, A. M., D’Onghia, E., Gottlöber, S., et al. 2008, *MNRAS*, 386, 2345
- Wetzel, A. R., Tinker, J. L., & Conroy, C. 2012, *MNRAS*, 424, 232
- Wyder, T. K., Treyer, M. A., Milliard, B., et al. 2005, *ApJL*, 619, L15
- Yoshida, M., Shimasaku, K., Kashikawa, N., et al. 2006, *ApJ*, 653, 988
- Yoshioka, T., Furuzawa, A., Takahashi, S., et al. 2004, *Advances in Space Research*, 34, 2525
- Zarattini, S., Girardi, M., Aguerri, J. A. L., et al. 2016, *A&A*, 586, A63
- Zheng, X. Z., Bell, E. F., Papovich, C., et al. 2007, *ApJL*, 661, L41
- Zibetti, S., Pierini, D., & Pratt, G. W. 2009, *MNRAS*, 392, 525